TESCE, October 2006, pp. 25-39

Modeling and Simulation of $LaNi_5$ Metal Hydride Reactor

Abeer Arafa[a], Tarek M. Moustafa[b] and Eman Bellah Metawee[a]

[a] Solar Energy Department, National Research Center, Dokki, Giza, Egypt
[b] Chemical Engineering Department, Faculty of Engineering, Cairo University, Giza, Egypt

Abstract

A one dimensional unsteady state mathematical model was developed for $LaNi_5$ metal hydride reactor. Kinetic equations for the absorption and desorption steps were included in the model. The simulation results of the model showed that heat transfer controls the overall rate of absorption and desorption. Near the reactor walls, maximum rate of the exothermic hydriding reaction was observed because of cooling. It was also observed that since the reaction is taking place in the solid phase, so the dynamics of the gas temperature is always lagging behind the solid temperature. The hydrogen pressure varies considerably along the reactor bed during the hydriding step at the beginning, while it levels towards the end of the reaction

1. Introduction

With rapid technical and industrial development all over the world, the need for energy sources is increased. Due to increase on fossil fuels dependency, thinking had started regarding its continuity especially with its destructive effect on environment and general health. Hydrogen is clean energy carrier and therefore is the best alternative. Hydrogen chemically bonded to metals and alloys at relatively low pressures and moderate temperature is completely reversible process. Metal hydride is the most compact method for hydrogen containment and it avoids many of the disadvantages of other means for hydrogen storage.

Metal hydride reactor is a complex system of simultaneous reaction, mass and heat transfer. The optimal conception of this installation requires the knowledge and the control of transient heat and mass transfer within the reactor during this absorption/desorption phenomena. Several models for the dynamic heat and mass transfer in metal hydride reactor have been developed in recent years [1, 2]. Most modeling studies assumed that the local gas and solid temperature were equal (local thermal equilibrium) [3-6], and that the convection term in an energy equation for gas phase was neglected [7].

Although there are several studies in the literature on the various aspects of the hydriding process, most of the models have been constructed without taking into consideration what is physically taking place in reality like bed volume increase and its effect on bed density. The purpose of this study is to extend the metal hydride reactor model and include the variation of the bed properties during the course of the reaction. This will lead to the accurate prediction of the

reactor performance and will ultimately yield to the optimization of its performance.

2. Mathematical model of hydride reactor

In the course of modeling of the hydride reactor, it was assumed that the cylindrical reactor exchanges heat through lateral and bases areas at a constant temperature fluid (Fig 1). The reactor is packed with $LaNi_5$ particle powders with an average diameter of 50 αm. The dimensions of the bed chosen for simulation are 60 mm in diameter, and 40 mm in height. The bed is not packed to the reactor top to allow free expansion of the metal hydride which will be formed during the reaction. A heterogeneous unsteady state one-dimensional model was used to describe the two phase reactor with the following assumptions:

- Hydrogen is assumed to behave as an ideal gas.
- The mass dispersion is often neglected.
- $LaNi_5$ particles have a spherical shape with a uniform diameter, and hence, the shape factor equals one.
- The bed porosity is constant every where.

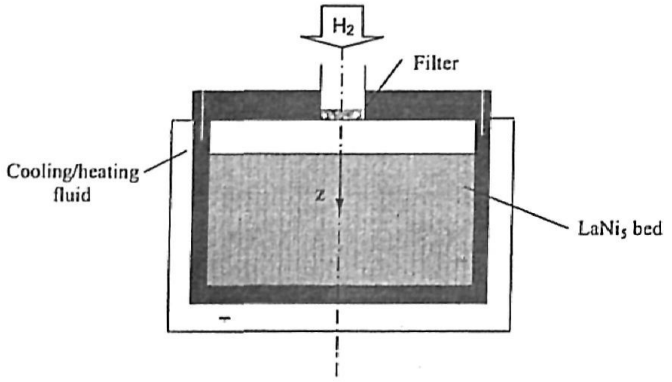

Fig. 1 Schematic View of the Reactor

2.1 Gas Phase Mass Balance

$$\varepsilon \frac{\partial \rho_g}{\partial t} + \frac{\partial \left(\rho_g u\right)}{\partial z} = -\dot{m} \qquad (1)$$

2.2 Gas Phase Energy Balance

$$\varepsilon Cp_g \rho_g \frac{\partial T_g}{\partial t} = -Cp_g \rho_g u \frac{\partial T_g}{\partial z} + \lambda_{geff} \frac{\partial^2 T_g}{\partial z^2} - h_{gs} a_p \left(T_g - T_s\right) \qquad (2)$$

2.3 Solid Phase Energy Balance

$$\left(1-\varepsilon\right) Cp_s \rho_s \frac{\partial T_s}{\partial t} = \lambda_{seff} \frac{\partial^2 T_s}{\partial z^2} + h_{gs} a_p \left(T_g - T_s\right) - \Delta H_r \dot{m} \qquad (3)$$

2.4 Momentum Balance Equation

Darcy's empirical law for laminar flow in porous media was used:

$$u = -\frac{K}{\propto}\frac{\partial P}{\partial z} \tag{4}$$

2.5 Initial and boundary conditions

Initial conditions and values employed in the simulation are shown in Table 1 and are also given by the following equations:

$$T_s(z,0) = T_f, \qquad T_g(z,0) = T_{go}, \qquad P(z,0) = P_o$$

Table 1 Initial condition for the model simulation

		Absorption	Desorption
P_o	atm	6.6	1.7
T_f	K	283	313
T_{go}	K	293	313
T_{so}	K	283	313

The heat flux continuity through lateral area and base area are expressed as:

$$-\lambda_i \frac{\partial T_i}{\partial z}(Z_o,t) = h_{wi}\left(T_i(Z_o,t) - T_f\right) \tag{5}$$

Where wall heat transfer coefficients (h_{ws} and h_{wg}) are given by Nakagawa et al. [9], assuming heat transfer is proportional to respective thermal conductivity of gas and solid, by:

$$h_{wi} = h_w \frac{\varepsilon_i \lambda_i}{\varepsilon_s \lambda_s + \varepsilon_g \lambda_g} \tag{6}$$

The pressure is assumed to be constant, and the gas temperature is assumed to be constant in absorption case and assumed to be equal to solid temperature in desorption case:

$$P(0,t) = P_o, \qquad T_g(0,t) = T_{go} \qquad \text{(absorption)}$$
$$P(0,t) = P_o \qquad T_g(0,t) = T_s(0,t) \quad \text{(desorption)}$$

The solid temperature at the inlet of the bed is tied by:

$$-\lambda_s \frac{\partial T_s}{\partial z}(0,t) = h_{gs}\left(T_{go} - T_s(0,t)\right) \tag{7}$$

The wall is impervious and therefore:

$$\frac{\partial P}{\partial z}(Z_o,t)=0 \tag{8}$$

3. Kinetic Model

$$M+\frac{x}{2}H_2 \Leftrightarrow MH_x$$

3.1 Kinetic Model for the Hydriding Reaction

For the hydriding kinetic, many studies for $LaNi_5$ system have reported an agreement between their experimental studies and both the shrinking core (SC) and nucleation and growth (NG) models. Based on most investigators [10- 12], the rate controlling step is initially nucleation and growth of the hydride phase and then becomes the hydrogen diffusion step through the hydride at a latter stage. In this study this kinetics was adopted and the governing equations of the kinetic model used as driven by Inomata et al. [12].

3.1.1 The nucleation and growth rate

$$K_1 = f(P,T)n(1-F)[-\ln(1-F)]^{\frac{n-1}{n}} \tag{9}$$

Where $f(P, T)$ is a function of pressure and temperature. Values of n = 3, and $f(P, T)= 0.072(P - P_{eq})$ were taken. The equilibrium pressure P_{eq} is given by the Van't Hoff's equation as a function of the solid temperature only, neglecting the effect of hydrogen concentration.

$$P_{eq} = \exp\left(A-\frac{B}{T_s}\right) \tag{10}$$

3.1.2 The hydrogen diffusion rate

$$K_2 = \frac{\tau}{\left((1-F)^{-1/3}-1\right)} \tag{11}$$

τ was found to be 5.278×10^{-3} $(P - P_{eq})$. By combining the two rates, the overall hydriding reaction rate is then given by:

$$\frac{dF}{dt} = \frac{1}{1/K_1 + 1/K_2} \tag{12}$$

3.2 Kinetic Model for the Dehydriding Reaction

Investigators in the literature [12] indicated that neither nucleation and growth process nor hydrogen diffusion through the hydride phase is the rate controlling step. The dehydriding reaction rate equation was thus expressed by:

$$\frac{dF}{dt} = k_1\left(P_{eq} - P\right)\left(1-F\right)^2 \tag{13}$$

3.3 Volumetric Rate of Reaction

In the hydriding/dehydriding reactions, the reaction rates are presented as a particle-volume fraction converted with time dF/dt as indicated in equations (12) and (13). For the $LaNi_5H_6$ system, the maximum hydrogen mass absorbed/desorbed per unit mass of alloy is about 0.0144 kg H_2/kg alloy, then we could present the volumetric reaction rate for this system as:

$$\dot{m} = 0.0144 \cdot \left(1-\varepsilon\right)\rho_s \cdot \frac{\partial F}{\partial t} \tag{14}$$

4. Thermo-physical and Hydrodynamic Parameters

Values for some thermophysical properties of materials and data used are summarized in Table 2, and other physical properties of solid phase are given as follows:

Table 2 Thermo-physical properties of materials and data used

		Absorption	Desorption
Cp_g	J/kgK	14420	14420
d_{p_o}	M	50×10^{-6}	53.8×10^{-6}
ΔH_r	J/kg	-15.1×10^6	15.43×10^6
λ_g	W/m K	0.18	0.18
ρ_{so}	Kg/m^3	4200	3394.7

4.1 Solid Density and Particle Diameter

$LaNi_5$ alloys are known to undergo a reversible volume expansion up to 25%, which has an effect on the particle diameter and the density of metal hydrides. Therefore, the particle diameter and the density of metal hydrides are expressed as:

$$d_p = d_{po}\left(1+\alpha F\right)^{1/3} \tag{15}$$

$$\rho_s = \rho_{so}\frac{1+\left(M_{H_2}/M_{alloy}\right)F}{\left(1+\alpha F\right)} \tag{16}$$

Where: α is a volume expansion coefficient and is taken to be 0.243 [9].

4.2 Specific Heat of Solid Phase

It is reported that the specific heat of alloys is varied with the absorption of hydrogen [1, 9, and 13]; therefore, it is necessary to take into account this change. The relation obtained by Nakagawa et al. [9], for the specific heat of metal hydrides was taken in this study.

$$Cp_s = \frac{\left(3.23R_g + 10.04 \cdot [H/M]_{max} F\right) \cdot 6 \cdot 1000}{M_{alloy} + 6 \cdot [H/M]_{max} F} \tag{17}$$

Where $[H/M]_{max}$ is the maximum atom ratio of hydrogen to alloy and it is equals 1.029 in case of $LaNi_5$. Cp_s given by the above equation increases almost linearly with an increase in reacted fraction.

4.3 Gas-to-Solid Heat Transfer Coefficient

There are several different correlations for the heat transfer coefficient between the solid particles and the fluid, which were used in the reactor models to calculate the temperature at the surface of the solids. Literature data on particle-to-fluid heat is rather consistent at values of Reynolds number larger than 500. At low Reynolds numbers, large differences can be observed. In our simulation Kunii's correlation [14] was used for particle-to-fluid heat transfer coefficient in packed beds of fine particles for low range of Peclet number, $Pe_p < 10$, which is typical for our case. Then, the Nusselt number is given as:

$$Nu_p = \frac{h_{gs} d_p}{\lambda_g} = \frac{\phi}{6(1-\varepsilon)\zeta} Pe_p \tag{18}$$

The Peclet number, Pe_p, equals:

$$Pe_p = \mathrm{Re.Pr} = \frac{\rho_g u d_p Cp_g}{\lambda_g} \tag{19}$$

Then, the heat transfer coefficient between gas and solid h_{gs} is given by the following equation:

$$h_{gs} = \frac{\rho_g u Cp_g \phi}{60(1-\varepsilon)} \tag{20}$$

5. Results and Discussion

5.1 Solution Methodology

In the mathematical model developed previously, systems of time-space dependent partial differential equations (PDEs) together with non-linear

algebraic equations have to be solved. The Method of Lines (MOL) was used to solve PDEs system by discretizing in space. The MOL solution process has two phases. In the first phase, the partial derivatives with respect to the independent spatial variables are replaced with algebraic approximations (finite difference) evaluated at discrete points. In the second phase, a series of time-dependent ordinary differential equations (ODEs) systems are solved using a dynamic integrator (Gear integrator which automatically varies the integration step and integration algorithm order). The accuracy of the approximate solution depends on the element spacing (for the axial domain) and the integration step size in time (0.1 sec). Using this element spacing, acceptable accuracy was achieved. The non-linear algebraic equations are solved with Newton method.

5.2 Simulation and model results

5.2.1 Absorption Process

During the absorption process, the exothermic hydriding reaction takes place. The dynamics of the bed was simulated the evolution of main reactor variables with time are presented as follows: the solid temperature distribution in the axial direction after 60 s, 1800 s, 4000 s, 6000 s, 7000 s, and 7500 s is presented in Fig 2. The temperature inside the reactor initially increases from to about 322 K due to the exothermic reaction then it decreases as the reaction rate decreases compared the rate of heat transfer from the bed to the jacket. Near the bottom, the temperature is less than in the interior of the reactor, due to the external fluid cooling from the jacket. After 6000 s, the alloy tends to reach hydrogen saturation; consequently, the heat released from the bed becomes too small. In this case the heat transfer limitation is mainly due to the stationary heat conduction inside the inert porous medium.

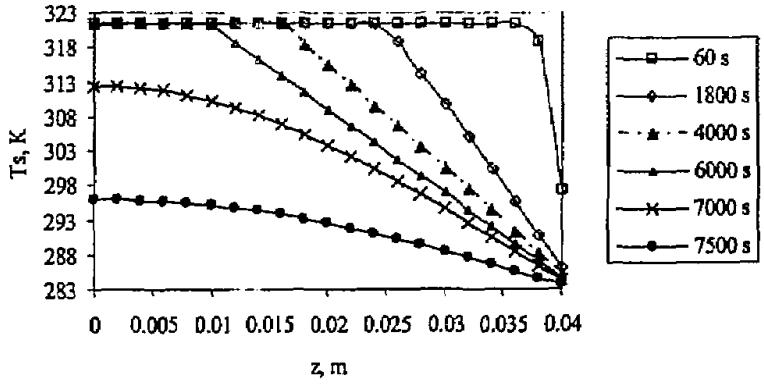

Fig. 2 Solid temperature distribution in the axial direction for absorption process at different times

The distribution of the gas temperature in the axial direction for the same time intervals is similar to the distribution of the solid temperature as shown in Fig.3. However, at the inlet of the reactor the hydrogen temperature distribution

is different from the solid temperature distribution because the inlet gas temperature was kept constant. Besides, the gas temperature is lagging behind the solid temperature because the exothermic reaction is taking place in the solid phase.

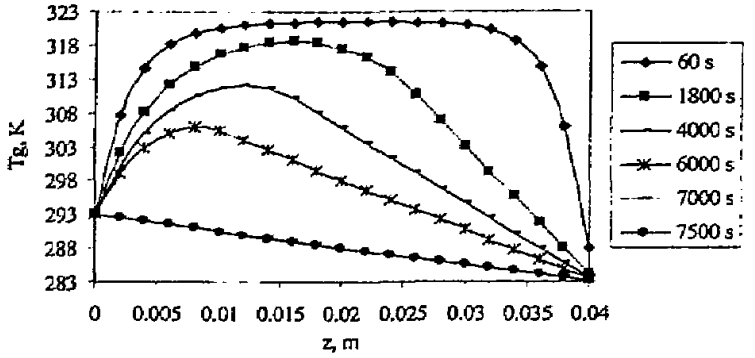

Fig. 3 Gas temperature distribution in the axial direction for absorption process at different times

Fig. 4 shows the evolution of pressure decrease inside the bed along the bed height (in terms of pressure difference) with time. The pressure decreases along the bed due to hydrogen consumption as well as bed resistance. After a long period of time, the alloy saturates and the pressure increases within the reactor and tends to be close to the inlet pressure (pressure difference values approaches zero). Gas superficial velocity, which is given in Fig. 5, was initially high (at t =60s) due to high rate of hydrogen absorption, then, it decreased as the alloy approached saturation. Also velocity trend shows a decrease along the bed height with the completion of the reaction and sharper near the bottom where the maximum rate of reaction is present due to highest heat removal.

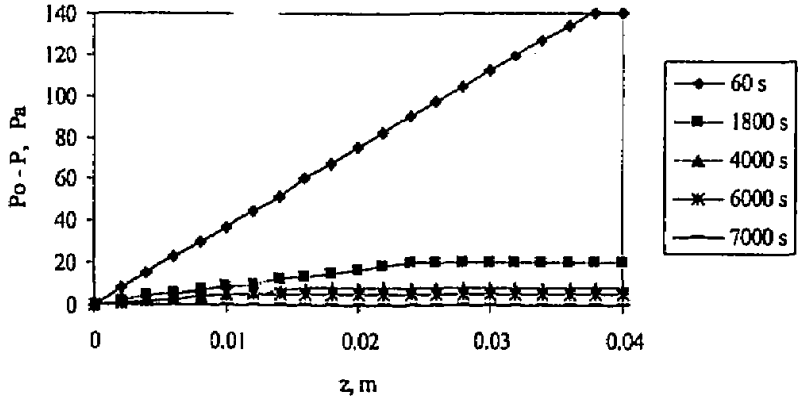

Fig. 4 Pressure difference distribution in the axial direction for absorption process at different times

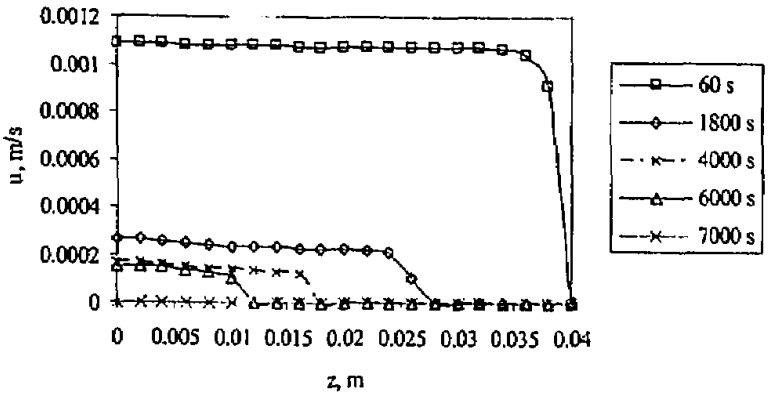

Fig. 5 Gas superficial velocity distribution in the axial direction for absorption process at different times

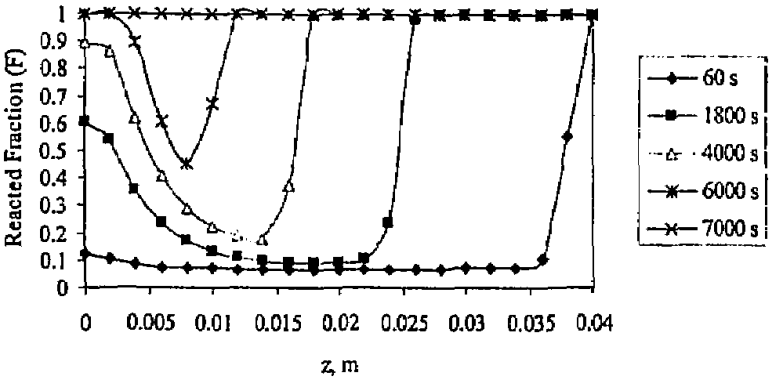

Fig. 6 Reacted fraction distribution in the axial direction for absorption process at different times

Fig. 6 shows the dynamic distribution of the reacted fraction along the bed height. It can be observed that the reaction proceeds mainly from the bottom and slightly from the top of the bed where the temperature is less than in the interior of the bed, so, the reaction rate is controlled by heat transfer.

Fig. 7 shows the performance of the hydride bed during absorption with different cooling fluid temperatures. It can be observed that as the cooling fluid temperature is reduced the average hydrogen absorbed mass increased. The reduction of the cooling fluid temperature will lead to lower average bed temperature which is favoring the reaction equilibrium.

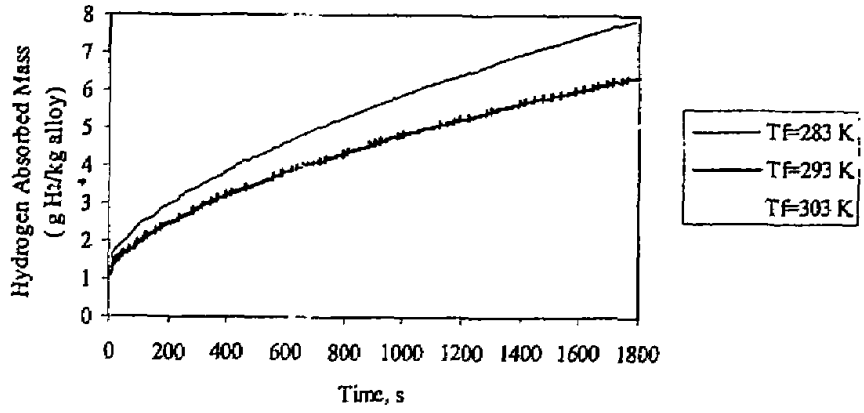

Fig. 7 Hydrogen absorbed mass during absorption at different cooling fluid temperatures

5.2.2 Desorption Process

Figures 8 and 9 show the evolution of solid and gas temperatures along bed height for desorption process at different times, t = 300, 1800, 2800, 4000, and 6000 s. Initially solid and gas temperatures are assumed to be as same as that of the heating fluid. The temperature profiles indicate that the temperature in the bed is significantly decreased due to the endothermic desorption reaction. However, the temperatures near the bottom of the bed remains higher as a result of heat supplied by the heating fluid. Both of the gas and solid temperatures increases with time because of the reaction rate decrease and heat supplied from the jacket.

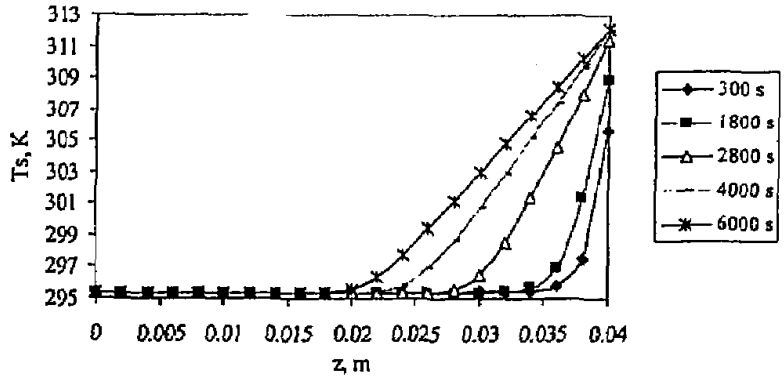

Fig. 8 Solid temperature profile in the axial direction for desorption process at different times

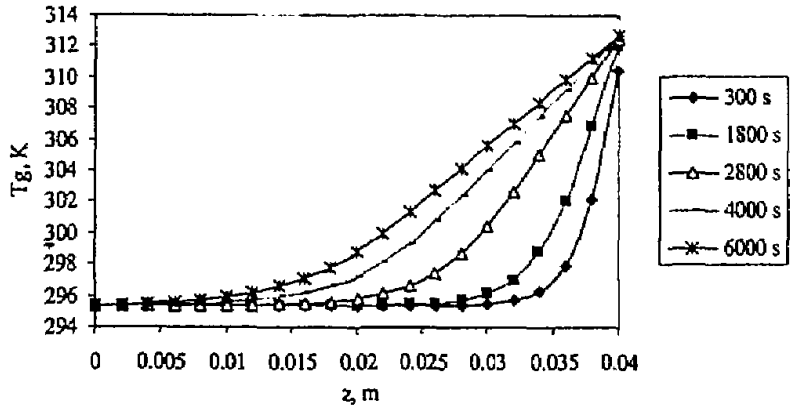

Fig. 9 Gas temperature profile in the axial direction for desorption process at different times

The pressure difference profiles along bed height at different times are shown in Fig. 10. Unlike the absorption case, the pressure in the bed increases due to the liberation of the hydrogen gas. Initially, this increase in pressure is high near the bottom of the bed as the reactions proceeds quickly due to the external fluid heating. The pressure difference profile decreased with time as the reaction tends to finish (the pressure in the bed tends to be the same as the outlet pressure).

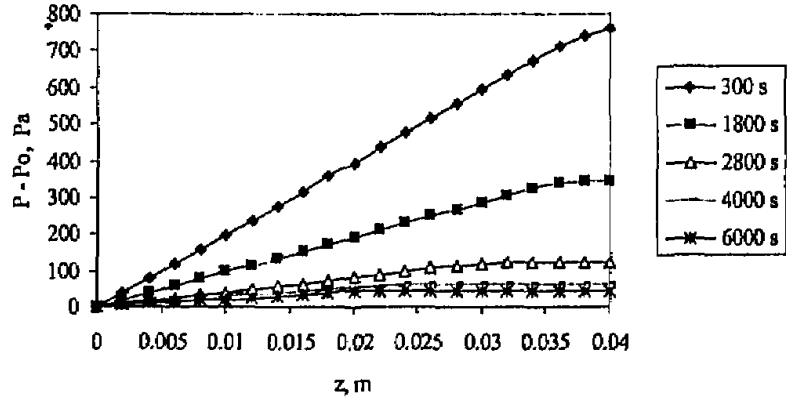

Fig. 10 Pressure difference profile in the axial direction for desorption process at different times

Fig. 11 shows the superficial velocity profiles at different times, t=300, 1800, 2800, 4000, and 6000 s. Initially, the gas velocity is high following the trend of the reaction which liberates high amount of hydrogen, then, the velocity decrease because the system reaches equilibrium.

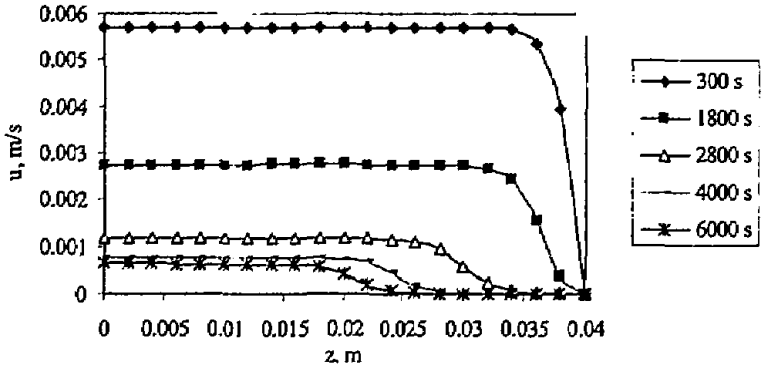

Fig. 11 Superficial gas velocity profile in the axial direction for desorption process at different times

Fig. 12 shows the reacted fraction profiles at different times, t=300, 1800, 2800, 4000, and 6000 s. The controlling parameter in dehydriding reaction is the equilibrium pressure which is a strong function of temperature. The reaction is faster near the bed bottom where heat is supplied, and thus higher temperature is reached. Initially dehydriding reaction increases rapidly and slows down when the bed gets cold due to the endothermic reaction.

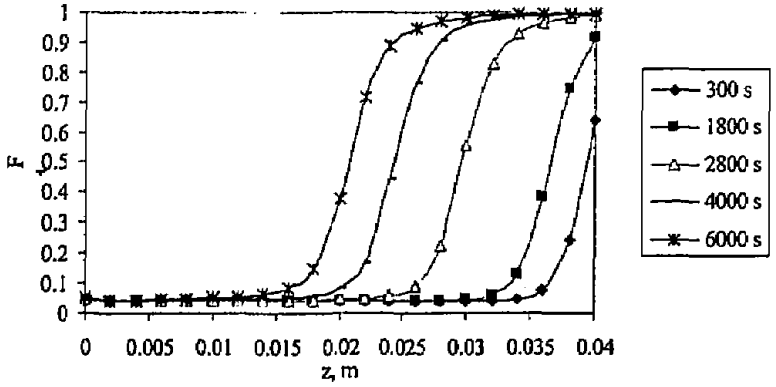

Fig. 12 Reacted fraction profile in the axial direction for desorption process at different times

6. Conclusions

The simulation results of the numerical one dimensional model revealed that both the absorption and desorption steps are highly controlled by heat transfer. Highest hydriding and dehydring reaction rates are encountered at the areas which are close to the cooling/heating jacket. Initially the hydriding reaction is highly affected by the applied hydrogen pressure, while towards the end of reaction the pressure difference along the bed is minimal. Reaction is taking

place mainly in the solid phase so the dynamics of the gas temperature is always lagging behind the solid temperature which is always higher in the exothermic hydriding reaction and lower in the dehydriding case. Since the cooling/heating effect near the side wall is critical, it might be worthy to take the radial temperature variation in consideration.

Nomenclature

a_p	Specific external surface area of the solid per unit reactor volume ($m^2\ m^{-3}$)
Cp	Specific heat Capacity ($J\ kg^{-1}\ K^{-1}$)
d_p	Particle diameter (m)
F	Reacted fraction
ΔH_r	Reaction heat ($J\ kg^{-1}$)
h_{gs}	Heat transfer coefficient between gas and solid ($W\ m^{-2}\ K^{-1}$)
h_w	Wall heat transfer coefficient ($W\ m^{-2}\ K^{-1}$)
H/M	Maximum atoms ratio of hydrogen to metal (mole $mole^{-1}$)
K	Permeability (m^2)
K_1	Absorption nucleation and growth rate (1/s)
K_2	Absorption hydrogen diffusion rate (1/s)
Nu_p	Nusselt number
M	Molecular weight ($kg\ kmole^{-1}$)
$\dot{m}$	Reaction volumetric rate ($kg\ m^{-3}\ s^{-1}$)
P	Gas pressure (Pa)
Pe_p	Peclet number
R_g	Gas constant ($J\ kmole^{-1}\ K^{-1}$)
T	Temperature (K)
t	Time (s)
u	Superficial gas velocity ($m\ s^{-1}$)
z	Axial coordinate (m)
Z_o	Hydride bed height (m)

Greek Symbols

α	Coefficient of volume expansion
ε	Porosity (m^3 void m^{-3} of bed)
λ	Thermal conductivity ($W\ m^{-1}\ K^{-1}$)
α	Viscosity (Pa s)
ρ	Density ($kg\ m^{-3}$)
ϕ	Shape factor

Subscripts

0	Initial
eff	Effective
eq	Equilibrium
F	Cooling/heating fluid
G	Gas
s	Solid

References

1. Choi, H., and Mills, A. F., "Heat and Mass Transfer in Metal Hydride Beds for Heat Pump Applications", International Journal of Heat and Mass Transfer, Vol. 33, pp. 1281-1288, 1990.

2. Gopal, M. R., and Murthy, S. S., "Prediction of Heat and Mass Transfer in Annular Cylindrical Metal Hydride Beds", International Journal of Hydrogen Energy, Vol. 17, pp. 795-805, 1992.

3. Isselhorst, A., "Heat and Mass Transfer in Coupled Hydride Reaction Beds", Journal of Alloys and Compounds, Vol. 231, pp. 871-879, 1995.

4. Jemni, A., Ben Nasrallah, S., and Lamloumi, J., "Experimental and Theoretical Study of a Metal-Hydrogen Reactor", International Journal of Hydrogen Energy, Vol. 24, pp. 520-533, 1999.

5. Mahmut, D., and Kaplan, Y., "Numerical Study of Hydrogen Absorption in an $LmNi_5$ Hydride Reactor", International Journal of Hydrogen Energy, Vol. 26, pp. 957–963, 2001.

6. Askri, F., Jemni, A., and Ben Nasrallah, S., "Dynamic Behavior of Metal–Hydrogen Reactor During Hydriding Process", International Journal of Hydrogen Energy, Vol. 29, pp. 635– 647, 2004.

7. Lee, S. G., Kim, T. G., and Lee, Z. H., "Mathematical Model for the Dynamic P-C-T Curves of the $MmNi_{4.6}Al_{0.2}Fe_{0.2}V_{0.03}$ Alloy in a Tubular Reactor", International Journal of Hydrogen Energy, Vol. 21, pp. 733-740, 1996.

8. Geankoplis, C. J., "Transport Processes and Unit Operation", Second Edition, Allyn and Bacon Series in Engineering, USA, ISBN 0-205-07788-9, 1983.

9. Nakagawa, T., Inomata, A., Aoki, H., and Miura, T., "Numerical Analysis of Heat and Mass Transfer Characteristics in the Metal Hydride Bed", International Journal of Hydrogen Energy, Vol. 25, pp. 339-350, 2000.

10. Han, J. I., and Lee, J. Y., "Hydriding Kinetics of $LaNi_5$ and $LaNi_{4.7}Al_{0.3}$", International Journal of Hydrogen Energy, Vol. 14, No. 3, pp. 181-186, 1989.

11. Osovizky, A., Bloch, J., Mintz, M. H., Jacob, I., "Kinetics of Hydride Formation in Massive $LaNi_5$ Samples", Journal of Alloys and Compounds, Vol. 35, pp. 168-178, 1996.

12. Inomata, A., Aoki, H., and Miura, T., "Measurement and Modeling of Hydriding and Dehydriding Kinetics", Journal of Alloys and Compounds, V. 278, pp. 103–109, 1998.

13. Dantzer, P., and Orgaz, E., "Thermodynamics of Hydride Chemical Heat Pump. How to Select a Pair of Alloys", International Journal of Hydrogen Energy, Vol. 11, pp. 797-806, 1986.

14. Kunii, D., and Suzuki, M., "Particle-to-Fluid Heat and Mass Transfer in Packed Beds of Fine Particles", International Journal of Heat and Mass Transfer, Vol. 10, pp. 845-852, 1967.